JOURNAL OF ENVIRONMENTAL SCIENCES 158 (2025) 337–350

Available online at www.sciencedirect.com

ScienceDirect

www.elsevier.com/locate/jes

JES JOURNAL OF ENVIRONMENTAL SCIENCES

www.jesc.ac.cn

Research Article

Comparative studies of the NO_x impacts on the photooxidation mechanisms of isomeric monoterpenes of β-pinene and limonene

Yingqi Zhao[1,2], *Zhaoyan Zhang*[1,2], *Ya Zhao*[1], *Chong Wang*[3,4], *Hua Xie*[1], *Jiayue Yang*[1], *Weiqing Zhang*[1], *Guorong Wu*[1], *Gang Li*[1,2,*], *Ling Jiang*[1,2,5,*], *Xueming Yang*[1,2,3,5,6]

[1] *State Key Laboratory of Molecular Reaction Dynamics and Dalian Coherent Light Source, Dalian Institute of Chemical Physics, Chinese Academy of Sciences, Dalian 116023, China*
[2] *University of Chinese Academy of Sciences, Beijing 100049, China*
[3] *Institute of Advanced Science Facilities, Shenzhen 518107, China*
[4] *Department of Chemical Physics, University of Science and Technology of China, Hefei 230026, China*
[5] *Hefei National Laboratory, Hefei 230088, China*
[6] *Department of Chemistry and Guangdong Provincial Key Laboratory of Catalytic Chemistry, Southern University of Science and Technology, Shenzhen 518055, China*

ARTICLE INFO

Article history:
Received 4 June 2024
Revised 30 July 2024
Accepted 4 August 2024
Available online 13 August 2024

Keywords:
Secondary organic aerosol
Anthropogenic–biogenic interactions
Photooxidation mechanism
β-pinene
Limonene

ABSTRACT

It is highly challenging to precisely compare the impacts of anthropogenic pollutants on the photooxidation of isomeric volatile organic compounds with respect to molecular compositions and particle number/mass concentrations of secondary organic aerosols (SOAs). In this study, we conducted a series of well-defined indoor chamber experiments to compare the effects of NO_x (NO and NO_2) on the photooxidation of isomeric monoterpenes of β-pinene and limonene. For the photooxidation of β-pinene with NO_x, the increase of the initial concentrations of NO ($[NO]_0$) shows a monotonous suppression of the particle mass concentration, whereas the increase of $[NO_2]_0$ shows a monotonous enhancement of the particle mass concentration. For the photooxidation of limonene with NO_x, the increase of $[NO]_0$ exhibits a monotonous suppression of the particle mass concentration, whereas the increase of $[NO_2]_0$ shows a parabolic trend of the particle mass concentration. Utilizing a newly developed vacuum ultraviolet free electron laser (VUV-FEL), the online threshold photoionization mass spectrometry reveals a series of novel compounds at molecular weight (MW) = 232 and 306 for the β-pinene + NO_x system and MW = 187, 261, 280, and 306 for the limonene + NO_x system. The molecular structures and formation pathways of these species were inferred, which led to the prediction of the diversity and difference of SOA products (i.e., ester and peroxide accretion products) formed from different monoterpene precursors.

* Corresponding authors.
E-mails: gli@dicp.ac.cn (G. Li), ljiang@dicp.ac.cn (L. Jiang).

https://doi.org/10.1016/j.jes.2024.08.007

To improve the predictions of future air quality, it is recommended that climate models should incorporate the NO_x-driven diurnal photooxidation of monoterpenes for SOA formation mechanisms.

Introduction

Secondary organic aerosols (SOA), primarily derived from the oxidative processes of biogenic precursors, constitute a significant fraction of the atmospheric aerosols in the troposphere, exerting substantial impacts on Earth's radiation balance, climate, and human health (Hallquist et al., 2009; Jimenez et al., 2009). Biogenic volatile organic compounds (BVOC), due to their large emissions and high reactivity, play a pivotal role in the formation of secondary pollutants (Wu et al., 2020). Laboratory and field studies indicate that the interaction between BVOCs and anthropogenic gases substantially alters the reaction characteristics of SOA formation, affording insights into the enhancement effects (Shilling et al., 2013; Xu et al., 2021, 2015; Yee et al., 2020). Understanding the interaction between BVOC and anthropogenic pollutants was proposed to be crucial for setting up effective atmospheric pollution control policies (Nagori et al., 2019).

Monoterpenes, featured by high emissions (> 100 Tg C/year) and high SOA yields, are significant contributors to global biogenic SOA (Engelhart et al., 2008). Recently, more and more laboratory and field studies focus on the significance of monoterpenes in the formation of SOA (Byron et al., 2022). β-pinene and limonene, released by plants, are the primary global contributors to monoterpenes and play a crucial role as precursors in the formation of SOA (Guenther et al., 2012). As isomers, β-pinene and limonene have identical molecular formula. As shown in Scheme 1, β-pinene possesses a double-ring configuration with an exocyclic double bond, whereas limonene possesses a single-ring structure with both an external and internal double bond with enhanced reactivity as compared to β-pinene (Grosjean et al., 1993; Liu et al., 2022). Consequently, limonene exhibits higher SOA yields as compared to β-pinene (Friedman and Farmer, 2018; Liu et al., 2022). Recent experimental studies have shown pronounced differences in the formation of highly oxygenated organic molecules (HOMs) and low-volatility compounds during the ozonolysis processes of β-pinene and limonene (Liu et al., 2022; Piletic and Kleindienst, 2022).

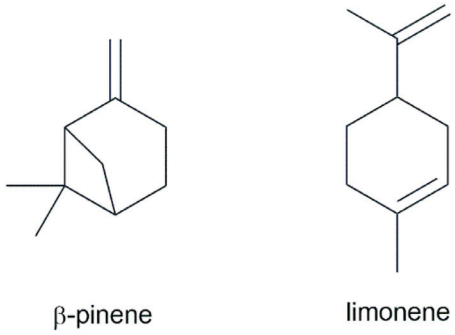

Scheme 1 – Structures of β-pinene and limonene.

As an important component of anthropogenic pollutants, NO_x has been proved to exhibit a great impact on the photooxidation of BVOC (Park et al., 2017; Sarrafzadeh et al., 2016; Zhao et al., 2018). In recent years, a large number of studies indicate that NO_x suppresses the formation of new particles, thereby inhibiting the condensation of low-volatility compounds onto the surfaces (Li et al., 2017; Wildt et al., 2014). NO_x directly influences the BVOC oxidation by altering the oxidant levels. Besides, there is also indirect influence of NO_x on the chemistry of RO_2, which further affects organic compound oxidation. However, there is a lack of comprehensive comparison of the impact of anthropogenic pollutants on the photooxidation of isomeric monoterpenes of β-pinene and limonene with respect to molecular compositions and particle number/mass concentrations of SOA.

HOMs were initially identified in forests, which are composed of six or more oxygen atoms that undergo autoxidation in the gaseous phase and play a crucial role in the growth of SOA (Bianchi et al., 2019; Tröstl et al., 2016). Numerous investigations have revealed the significance of HOMs in the formation and growth of new particles (Bianchi et al., 2016; Jokinen et al., 2014; McFiggans et al., 2019). HOMs could be formed through an intramolecular hydrogen-atom shift (H-shift) within peroxyl radicals and their subsequent reaction with molecular oxygen (Bianchi et al., 2019; Crounse et al., 2013). The longevity of peroxyl radicals facilitates consecutive H-shift during the autoxidation processes. Considering the variation of products, lifetimes, and reactivity of HOMs in different types of SOA, it is essential to distinguish the compositional characteristics. Much efforts have been made on the formation of HOMs through the OH- and O_3-induced oxidation of monoterpenes, such as α-pinene, β-pinene, and limonene (Berndt et al., 2016; Kirkby et al., 2016; Luo et al., 2023; Shen et al., 2022; Xu et al., 2022). Given the persistently worsening NO_x pollution, it is of vital importance to explore deeply into the interrelationships between NO_x concentrations, BVOC types, and HOMs distributions, as well as the NO_x-dependent mechanisms for SOA and HOMs formation.

The objective of this study is to compare the distinct impacts of NO_x concentration on the size distribution, number concentration, mass concentration, and chemical composition of SOA formed through the photooxidation of β-pinene and limonene. Utilizing the aerosol mass spectrometry based on near-threshold photoionization using a tunable vacuum ultraviolet free electron laser (VUV-FEL), the chemical compositions of SOA were systematically analyzed. Using quantum chemical computations, we proposed plausible formation mechanisms for the newly observed products, highlighting the pivotal role of oxygen-based peroxy radical chemistry in the formation of HOMs. Our study shows that incorporat-

ing the NO_x concentration-driven monoterpene SOA formation and evolution mechanisms into future climate models would lead to more accurate air quality predictions and management.

1. Materials and methods

The experiments were conducted within a 2 m^3 indoor smog chamber at the Dalian Institute of Chemical Physics, Chinese Academy of Sciences (DICP-CAS) (Zang et al., 2022). A brief overview of experimental methods is provided here, with a more detailed description available in previous research (Zang et al., 2022) and in Appendix Supplementary data. In this work, β-pinene (99 %, Aladdin) or limonene (99 %, Aladdin) were used as primary BVOC precursors, which were introduced into the chamber through an airline. The photooxidation experiments were carried out under 40 black lamps (General Electric Company, USA). Prior to each experiment, the chamber was rigorously cleaned using an automated system, which employed a multi-step process of air condensation, freeze-drying, and catalytic adsorption to ensure zero air output with relative humidity (RH) below 3 % to ensure optimal conditions. The temperature of the chamber was held constantly at approximate 24.0 °C with a thermostatically controlled air conditioner prior to the commencement of the experiment.

The concentrations of nitrogen oxides (NO, NO_2, and NO_x) were determined using a gas analyzer (Model 42i, Thermo Fisher Scientific, UK). O_3 was formed from photochemical reactions of NO_x. The O_3 levels were measured by another gas analyzer (Model 49i, Thermo Fisher Scientific, UK). The VOCs were analyzed employing a proton-transfer reaction mass spectrometry (PTR-QMS 3500, East & West Analytical Instruments, China). Particle number concentrations, mass concentrations, and size distributions were measured using a scanning mobility particle sizer (SMPS 3938NL76; TSI Incorporated, USA). The preassigned particle density of 1.0 g/cm^3 was used to convert volume concentrations to mass concentrations. The uncertainty of mass concentrations measured by SMPS was estimated to be < 2.0 % by repeating the measurement of the 369 ppb limonene + 94 ppb NO_2 photooxidation reaction (Appendix A Fig. S1).

The particles generated in the DICP-CAS chamber were transported through a silicone tube to the time-of-flight aerosol mass spectrometer (TOF-AMS) using VUV-FEL for ionization. The VUV-FEL TOF-AMS employed an aerodynamic lens system to introduce aerosols from atmospheric pressure onto a copper rod mounted a high vacuum mass spectrometer (Wang et al., 2005; Zang et al., 2022). The deposited particles were vaporized by using a cartridge heater, ionized by VUV-FEL, and detected by TOF-MS in positive ion mode. Our TOF-MS was calibrated by a series of standard organic compounds (i.e., vanillin, 1-pentadecanol, n-Eicosane, etc.). The comparison of mass spectra of heater ON and OFF indicated that the ionization of gas-phase products had a negligible interference on the ionization of particles. The threshold photoionization

Table 1 – The experimental conditions of β-pinene + NO/NO_2 and limonene + NO/NO_2 photooxidation.

VOC	$[VOC]_0$ (ppb)	$[NO]_0$ (ppb)	$[NO_2]_0$ (ppb)	$[NO_x]_0$ (ppb)	$[VOC]_0$ /$[NO_x]_0$	ΔM (μg/m^3)	ΔROG (ppb)	SOA Yield (%)
β-pinene	333	0	45	45	7.4	170	302	10.1
β-pinene	369	1	118	119	3.1	333	316	19.0
β-pinene	381	1	165	166	2.3	384	335	20.7
β-pinene	358	5	285	290	1.2	566	308	33.1
β-pinene	341	5	357	362	0.9	697	325	38.7
β-pinene	339	46	0	46	7.4	118	310	6.9
β-pinene	360	120	2	122	3.0	104	322	5.8
β-pinene	389	163	1	164	2.4	101	329	5.5
β-pinene	377	263	0	263	1.4	108	370	5.3
β-pinene	365	358	9	367	1.0	10	355	0.5
β-pinene	970	0	401	401	2.4	857	868	17.8
β-pinene	976	397	6	403	2.4	654	856	13.9
β-pinene	2381	8	429	437	5.4	1943	1973	17.8
limonene	360	0	52	52	7.0	1168	334	63.1
limonene	364	0	98	98	3.7	1240	343	65.2
limonene	361	0	192	192	1.9	1363	336	73.2
limonene	388	1	252	253	1.5	1521	363	75.6
limonene	347	2	367	369	0.9	1048	315	60.0
limonene	375	51	3	54	7.0	1094	334	59.1
limonene	369	94	5	99	3.7	897	325	49.8
limonene	381	185	9	194	2.0	396	365	19.6
limonene	358	246	17	263	1.4	121	332	6.6
limonene	341	347	10	357	1.0	79	319	4.5
limonene	991	0	395	395	2.5	1726	954	32.6
limonene	982	399	7	406	2.4	1689	947	32.2
limonene	2230	9	373	382	5.4	2605	1960	24.0

$[x]_0$ stands for initial concentration in the smog chamber and ΔM for particle mass concentration. ΔROG stands for the amount of reacted organic gas.

of molecule was achieved by using the tunable VUV-FEL to lose an electron to produce a molecular ion M^+. The positions of mass spectral peaks detected in this work denote the molecular weight (MW) values. Our VUV-FEL TOF-AMS is able to detect the main size distributions of particles, ranging from 30 to 2500 nm and detect particle-phase products in real-time. The threshold ionization of neutral compounds was realized by taking advantage of high selectivity via the widely tunable wavelength range of VUV-FEL (50–150 nm/8.3–24.8 eV) and high detection sensitivity of trace species via the high pulse energy (~ 100 μJ) (Zang et al., 2022; Zhang et al., 2024, 2025).

In order to understand the experimental results and to study the photooxidation mechanisms of β-pinene and limonene, quantum chemical calculations were performed at the ωB97XD/def2-TZVP level of theory employing the Gaussian 16 computational chemistry software package (Frisch et al., 2016). Transition states (TSs) were subjected to a thorough optimization employing the Berny algorithm, and their integrity was further corroborated by rigorous intrinsic reaction coordinate (IRC) computations. The relative energies were refined by incorporating the zero-point vibrational energy (ZPVE) corrections.

2. Results and discussion

A series of smog chamber experiments were conducted to extensively investigate the photooxidation systems of β-pinene + NO_x and limonene + NO_x (Table 1), with the primary objective of examining the specific effects of NO_x on secondary aerosol formation under various photochemical conditions. In the previous monoterpene experiments, high VOC concentrations of ~300 ppb (Hanson et al., 2022; Iinuma et al., 2007; Zang et al., 2024) and ~1000 ppb (Park et al., 2017) have

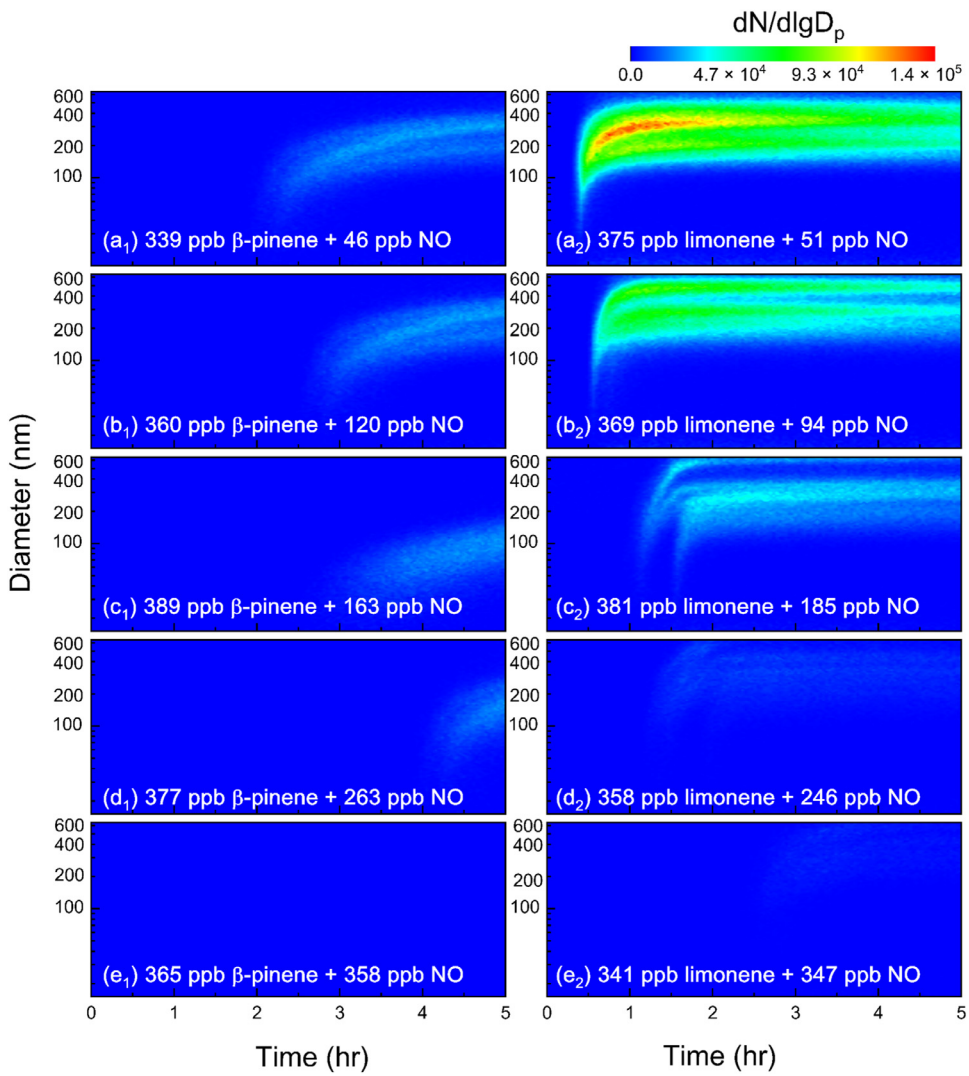

Fig. 1 – Temporal evolution of the particle size distribution in the photooxidation experiment based on $[NO]_0$ as the main variable at experimental conditions of (a_1) 339 ppb β-pinene + 46 ppb NO; (b_1) 360 ppb β-pinene + 120 ppb NO; (c_1) 389 ppb β-pinene + 163 ppb NO; (d_1) 377 ppb β-pinene + 263 ppb NO; (e_1) 365 ppb β-pinene + 358 ppb NO; (a_2) 375 ppb limonene + 51 ppb NO; (b_2) 369 ppb limonene + 94 ppb NO; (c_2) 381 ppb limonene + 185 ppb NO; (d_2) 358 ppb limonene + 246 ppb NO; (e_2) 341 ppb limonene + 347 ppb NO. D_p: particle diameter; dN/dlgD_p: normalized number size distribution.

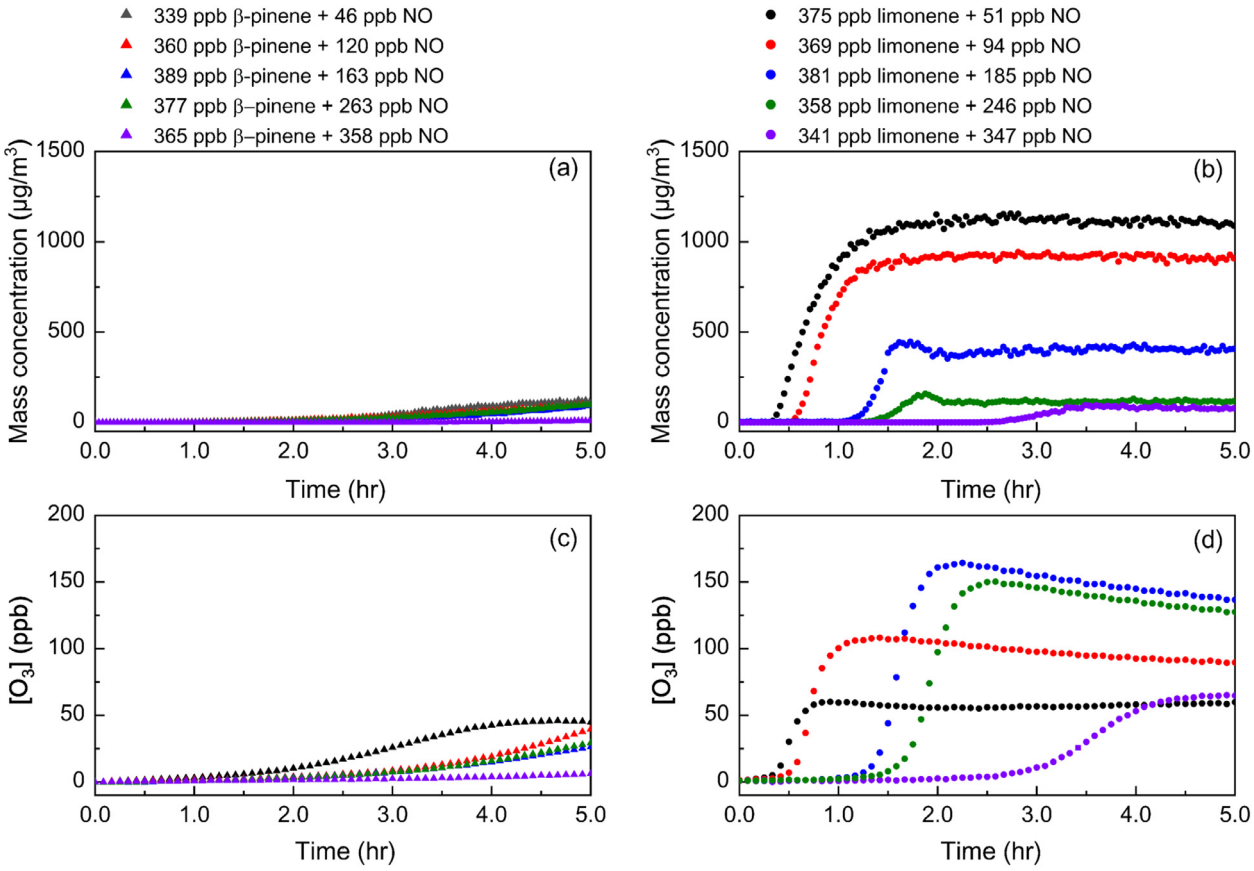

Fig. 2 – The particle mass concentration and O_3 concentration as a function of $[NO]_0$. The triangles and dots denote the β-pinene + NO experiments (a and c) and the limonene + NO experiments (b and d), respectively.

been used to ensure that the concentrations of particles are sufficient for accurate measurement. The isoprene concentration (100–1250 ppb) and NO_x concentration (50–600 ppb) have been set to investigate isoprene photooxidation (Zhang et al., 2011). The concentrations of 2000–4000 ppb for β-pinene and 1000–3000 ppb for limonene have also been used (Liu et al., 2022). In this work, we have selected the mixing of VOCs (300–2230 ppb) and NO_x concentration (45–406 ppb) to study the NO_x impacts on the photooxidation mechanisms of isomeric monoterpenes of β-pinene and limonene.

2.1. *Effects of $[NO]_0$ and $[NO_2]_0$ on particle size distribution, number and mass concentrations*

The impacts of the initial concentration of NO ($[NO]_0$) on the size distribution of particles formed by the β-pinene and limonene photooxidation reactions are illustrated in Fig. 1. As shown in Fig. 1a$_1$ and a$_2$, the nucleation time for the β-pinene system is 2 h in the 339 ppb β-pinene + 46 ppb NO reaction, while that for limonene is only 25 min in the 375 ppb limonene + 51 ppb NO reaction, indicating that the nucleation process in the limonene + NO photooxidation reaction is remarkably faster than that in the β-pinene + NO photooxidation reaction. Since limonene possesses a single-ring structure with both an external and internal double bond that exhibits higher reactivity than β-pinene (Scheme 1), this structure may result in a faster reaction rate towards oxidation (Appendix A Table S1) (Ehn et al., 2014) and the formation of highly volatile products (Liu et al., 2022). As the $[NO]_0$ gradually increases, the number concentrations of SOA formed from both the β-pinene and limonene systems gradually decrease (Fig. 1a$_1$-e$_1$, 1a$_2$-e$_2$). These results indicate that NO suppresses the SOA formation, which could alter the fate of RO_2 radicals generated during VOC oxidation, lead to the formation of organic nitrates, and subsequently change the distribution of photooxidation reaction products. Such features are in line with previous studies (Chen et al., 2022; Sarrafzadeh et al., 2016; Wildt et al., 2014).

The temporal evolution of particle mass concentrations and O_3 concentrations in the β-pinene + NO and limonene + NO photooxidation experiments is illustrated in Fig. 2. The increase of $[NO]_0$ shows a slight suppression of particle mass concentration throughout the photooxidation reaction of β-pinene with NO (Fig. 2a). However, in the limonene + NO photooxidation experiments, as the $[NO]_0$ increases, there is a notably stronger suppression of particle mass concentration by influencing peroxyl radical chemistry (Fig. 2b). Therefore, the dependency of SOA formation on $[NO]_0$ varies across different chemical systems. For photooxidation reaction of 381 ppb limonene + 185 ppb NO (Fig. 2d), the cu-

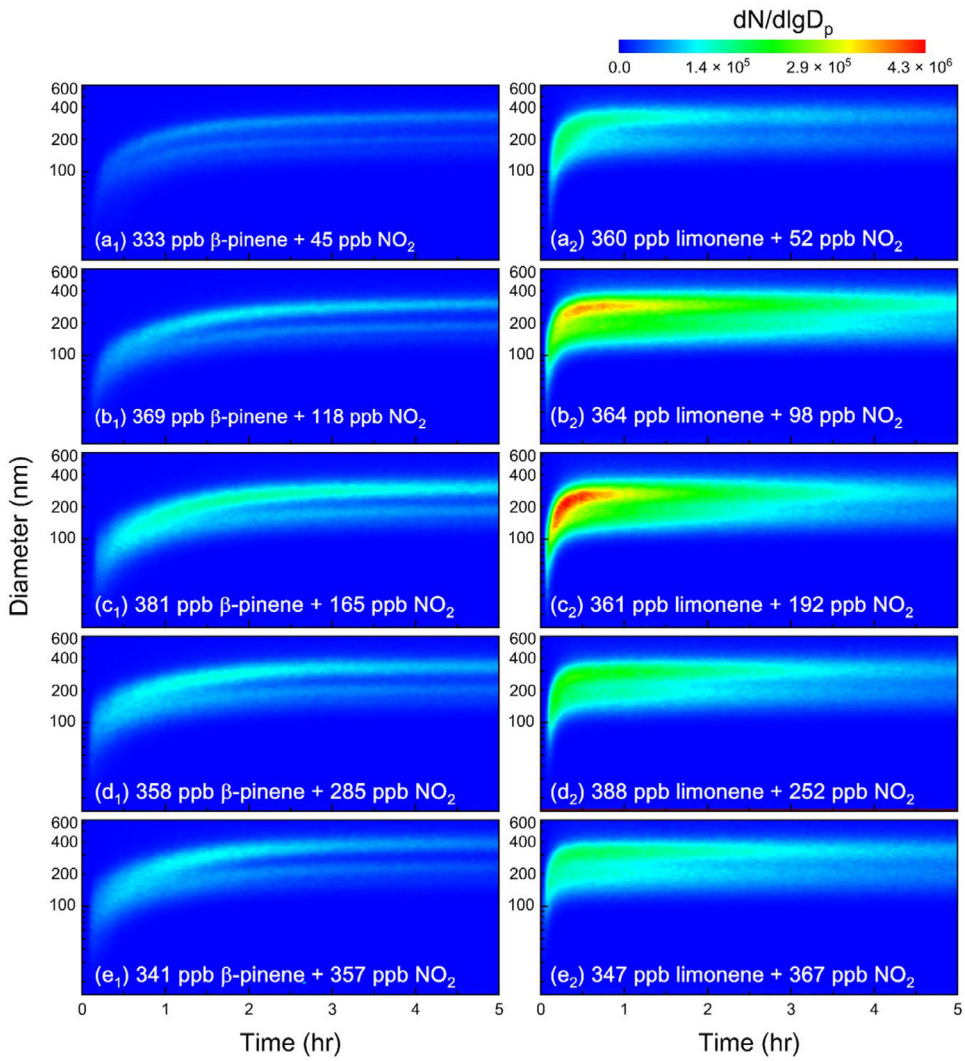

Fig. 3 – Temporal evolution of the particle size distribution in the photooxidation experiment based on $[NO_2]_0$ as the main variable at experimental conditions of (a_1) 333 ppb β-pinene + 45 ppb NO_2; (b_1) 369 ppb β-pinene + 118 ppb NO_2; (c_1) 381 ppb β-pinene + 165 ppb NO_2; (d_1) 358 ppb β-pinene + 285 ppb NO_2; (e_1) 341 ppb β-pinene + 357 ppb NO_2; (a_2) 360 ppb limonene + 52 ppb NO_2; (b_2) 364 ppb limonene + 98 ppb NO_2; (c_2) 361 ppb limonene + 192 ppb NO_2; (d_2) 388 ppb limonene + 252 ppb NO_2; (e_2) 347 ppb limonene + 367 ppb NO_2. D_p: particle diameter; $dN/dlgD_p$: normalized number size distribution.

mulative O_3 concentration is the highest, and two nucleation events are observed in Fig. 1c$_2$, indicative of a possible change in reaction pathway. The cumulative change in the O_3 concentration might influence the extent of the O_3 reactions with double bond of limonene, thereby affecting the types and yields of the products.

The formation of O_3 in the atmosphere is a complex chemical process (Wang et al., 2017). During the daytime, atmospheric oxidation of monoterpene is primarily driven by the interactions with NO_x, in which the NO_x photolysis plays a significant role in the generation of O_3. The consequence of this process depends on the concentration of the oxidant and the reactivity of the monoterpene. As depicted in Fig. 2c, for the photooxidation reaction of β-pinene with NO, an increase in the $[NO]_0$ leads to a decrease in the O_3 accumulation. In the limonene + NO photooxidation reaction (Fig. 2d), the O_3 accumulation initially rises with increasing $[NO]_0$ to 185 ppb, but slows down as $[NO]_0$ levels continue to rise. These contrasting responses observed for β-pinene and limonene could be attributed to the limonene's enhanced reactivity with O_3 (Appendix A Table S1), which accelerates the production of RO_2 and subsequently enhances the conversion of NO to NO_2, which in turn facilitates the O_3 accumulation. These findings are in line with the nonlinear variation of ground-level O_3 concentrations of NO levels (Liu and Shi, 2021).

Fig. 3 illustrates the particle size distribution of β-pinene and limonene photooxidation as a function of $[NO_2]_0$. As shown in Fig. 3a$_1$-e$_1$, in the β-pinene + NO_2 photooxidation reactions, as the $[NO_2]_0$ increases, particle number concentration gradually rises. In the limonene + NO_2 photooxidation reactions (Fig. 3a$_2$-e$_2$), as the $[NO_2]_0$ increases to 192 ppb, the particle number concentration significantly rises, but as the

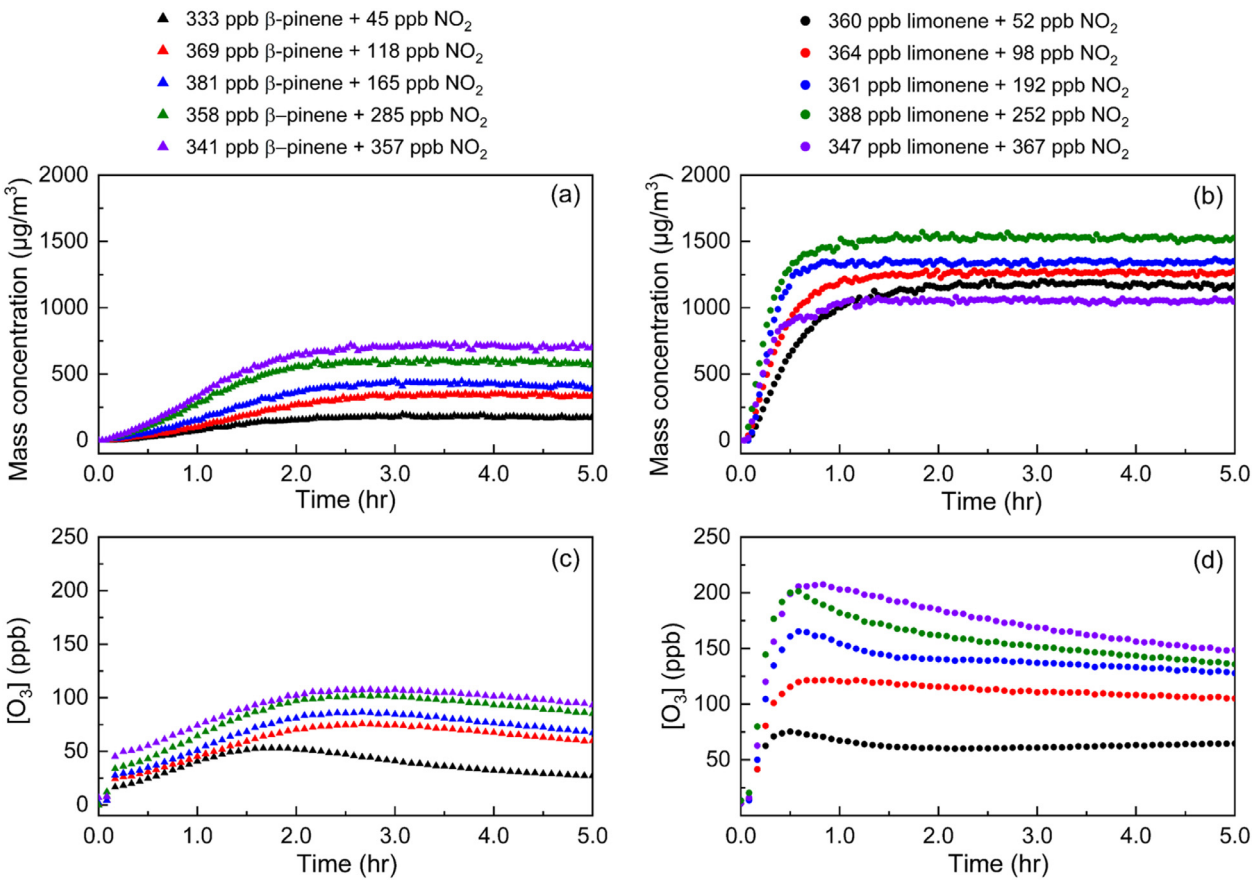

Fig. 4 – The particle mass concentration and O_3 concentration as a function of $[NO_2]_0$. The triangles and dots represent the β-pinene + NO_2 experiments (a and c) and the limonene + NO_2 experiments (b and d), respectively.

$[NO_2]_0$ continues to rise, it exhibits a pronounced suppression effect on particle number concentration. The key difference between limonene + NO_2 and β-pinene + NO_2 photooxidation reactions is ascribed to higher reactivity of limonene (preference of more RO_2 radical formation) as compared to β-pinene. The pronounced suppression effect on the photooxidation of limonene under the conditions of $[NO_2]_0 > 192$ ppb could be due to the reaction of RO_2 and NO produced by NO_2 photolysis. At a given $[NO_2]_0$, the particle size distribution of SOA formed from the limonene + NO_2 photooxidation (Fig. 3a_2-e_2) exhibits a broader range than that of SOA formed from the β-pinene + NO_2 photooxidation (Fig. 3a_1-e_1), which is reminiscent of the broader size distribution range of SOA from the limonene ozonolysis than that from the β-pinene ozonolysis (Liu et al., 2022). Such difference in the size distribution and particle number concentration for β-pinene or limonene may be related to the distribution of low volatile organic compounds, thus promoting the formation and growth of molecular clusters. Our results are supported by previously-observed high yields of extremely low-volatility organic compounds (ELVOCs) in the atmospheric oxidation of limonene (Hanson et al., 2022; Liu et al., 2022; Piletic and Kleindienst, 2022).

Photolysis of NO_2 is the main pathway for the O_3 generation in the troposphere, which directly affects the O_3 concentrations and subsequently affects atmospheric oxidation and photochemical processes (Tao et al., 2014). In the β-pinene + NO_2 photooxidation reactions, as the $[NO_2]_0$ rises, the O_3 concentration generated from the NO_2 photolysis increases (Fig. 4c and Appendix A Fig. S2a_1-e_1), concurrently with an increase in the particle mass concentration (Fig. 4a). In the limonene + NO_2 photooxidation reactions, as the $[NO_2]_0$ increases to 252 ppb, due to the increasing accumulation of O_3 (Fig. 4d and Appendix A Fig. S2a_2-e_2), particle mass concentration also exhibits a similar increasing trend (Fig. 4b). However, as $[NO_2]_0$ increases to 367 ppb, particle mass concentration decreases (Fig. 4b), which is linked to the suppression effect of RO_2 formation by NO generated through the photolysis of NO_2. Since the time of O_3 cumulative peak (Fig. 4c and d) generally coincides with the time when mass concentration reaches its maximum (Fig. 4a and b), it can be inferred that O_3 triggers an increase in the mass concentration of β-pinene and limonene photooxidation reaction products. In the limonene + NO_2 photooxidation reaction, O_3 reaches its maximum at approximately 0.5 h (Fig. 4d), whereas for the β-pinene + NO_2 photooxidation reaction (Fig. 4c), O_3 reaches its maximum at approximately 2 h, which indicates that the rate of O_3 formation in the limonene photooxidation process is faster. As compared to the β-pinene + NO_2 photooxidation reactions (Fig. 4a and Appendix A Fig. S3), the higher mass concentration of the limonene + NO_2 photooxidation (Fig. 4b and Appendix A Fig. S3) might be attributed to the unique chemical structure and reaction characteristics of limonene, as well

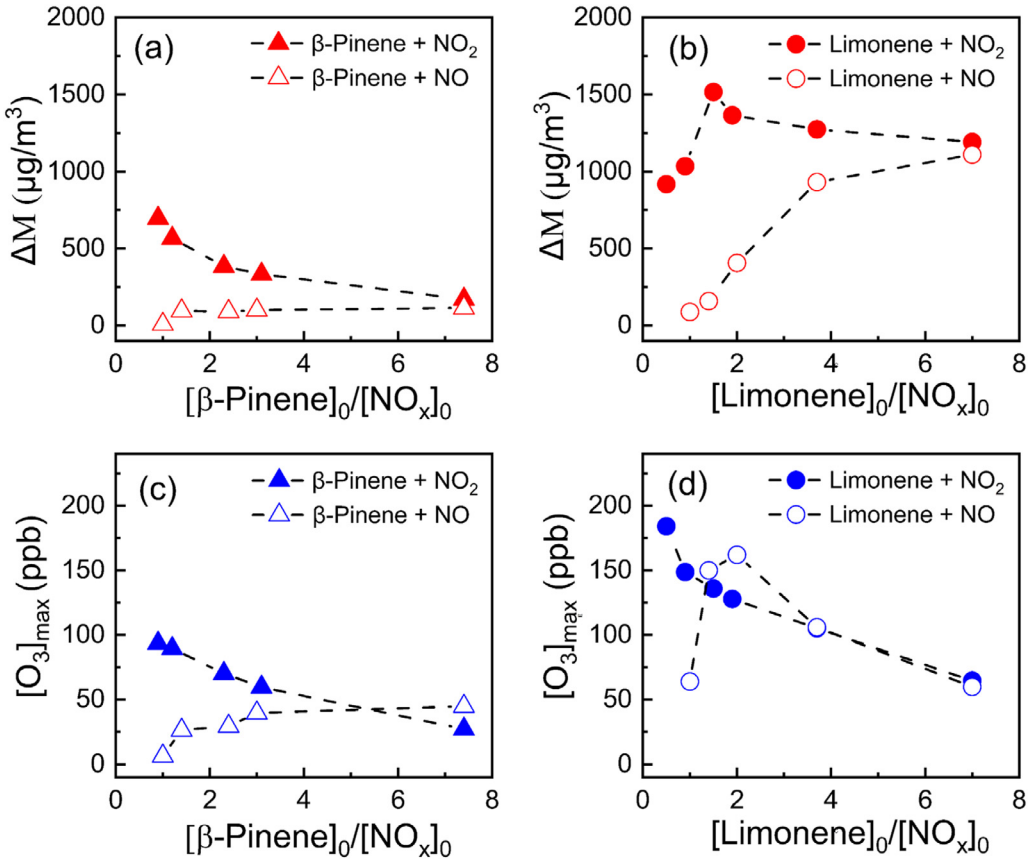

Fig. 5 – The particle mass concentration (ΔM) and O_3 maximum concentration ($[O_3]_{max}$) as a function of $[\beta\text{-pinene}]_0/[NO]_0$, $[\beta\text{-pinene}]_0/[NO_2]_0$, $[\text{limonene}]_0/[NO]_0$, and $[\text{limonene}]_0/[NO_2]_0$.

as the faster rates of O_3 formation from NO_2 photolysis (Fig. 4c and d).

While previous studies have examined the impact of the $[\beta\text{-pinene}]_0/[NO_x]_0$ and $[\text{limonene}]_0/[NO_x]_0$ ratios on the SOA formation (Liu and Shi, 2021), the specific effects of the $[\beta\text{-pinene}]_0/[NO]_0$, $[\beta\text{-pinene}]_0/[NO_2]_0$, $[\text{limonene}]_0/[NO]_0$, and $[\text{limonene}]_0/[NO_2]_0$ ratios remain unexplored. Hence, the dependence of particle mass concentration, O_3 maximum concentration, and SOA yields on the $[\beta\text{-pinene}]_0/[NO]_0$, $[\beta\text{-pinene}]_0/[NO_2]_0$, $[\text{limonene}]_0/[NO]_0$, and $[\text{limonene}]_0/[NO_2]_0$ has been studied and the results are illustrated in Fig. 5 and Appendix A Fig. S4, respectively. For the β-pinene + NO_x photooxidation reactions, as the $[\beta\text{-pinene}]_0/[NO]_0$ ratio increases, the particle mass concentration increases slightly (Fig. 5a), which trend holds true for the O_3 accumulation (Fig. 5c). In contrast, the particle mass concentration and O_3 maximum concentration decrease with the increase of the $[\beta\text{-pinene}]_0/[NO_2]_0$ ratio (Fig. 5a and c). For the limonene + NO photooxidation reactions, the particle mass concentration remarkably increases with increasing the $[\text{limonene}]_0/[NO]_0$ ratio from 0.9 to 3.7 and slightly increases with further increasing the $[\text{limonene}]_0/[NO]_0$ ratio to 7.0 (Fig. 5b), revealing a more pronounced suppression effect of NO on the limonene photooxidation than that on the β-pinene photooxidation. Note that the reaction of NO with the RO_2 radical could form a stable $RONO_2$ product, which consumes the RO_2 radical and thereby inhibits the autoxidation process. The aforementioned different effects of the $[\beta\text{-pinene}]_0/[NO]_0$ and $[\text{limonene}]_0/[NO]_0$ ratios on the SOA formation could be rationalized that the reaction of NO with the RO_2 radicals generated from limonene is more readily than that with the RO_2 radicals generated from β-pinene. The effect of $[\text{limonene}]_0/[NO_2]_0$ on the cumulative O_3 concentration (Fig. 5d) is also more pronounced than $[\beta\text{-pinene}]_0/[NO_2]_0$ (Fig. 5c). Such difference in the response of O_3 formation from β-pinene and limonene provides a reference for studies on the nonlinear relationship O_3 formation to various precursors in real atmospheric conditions (Liu and Shi, 2021; Sillman, 1999).

2.2. *VUV-FEL photoionization mass spectra of β-pinene and limonene photooxidation*

In this study, chemical compositions of the compounds formed from the β-pinene + NO/NO_2 and limonene + NO/NO_2 photooxidation processes were measured using a VUV-FEL photoionization aerosol mass spectrometer. Previous studies have shown that by optimizing the VUV-FEL wavelengths and pulse energies, the threshold photoionization can be achieved with high sensitivity, high selectivity, and negligible fragmentation (Normile, 2017; Zang et al., 2022; Zhang et al., 2024, 2025). Our prior studies indicated that reaction times for terpenes and NO_x at slightly higher concentrations can be remarkably reduced without significant variation of chemical compositions of SOA (Zang et al., 2022; Zhang et al., 2024,

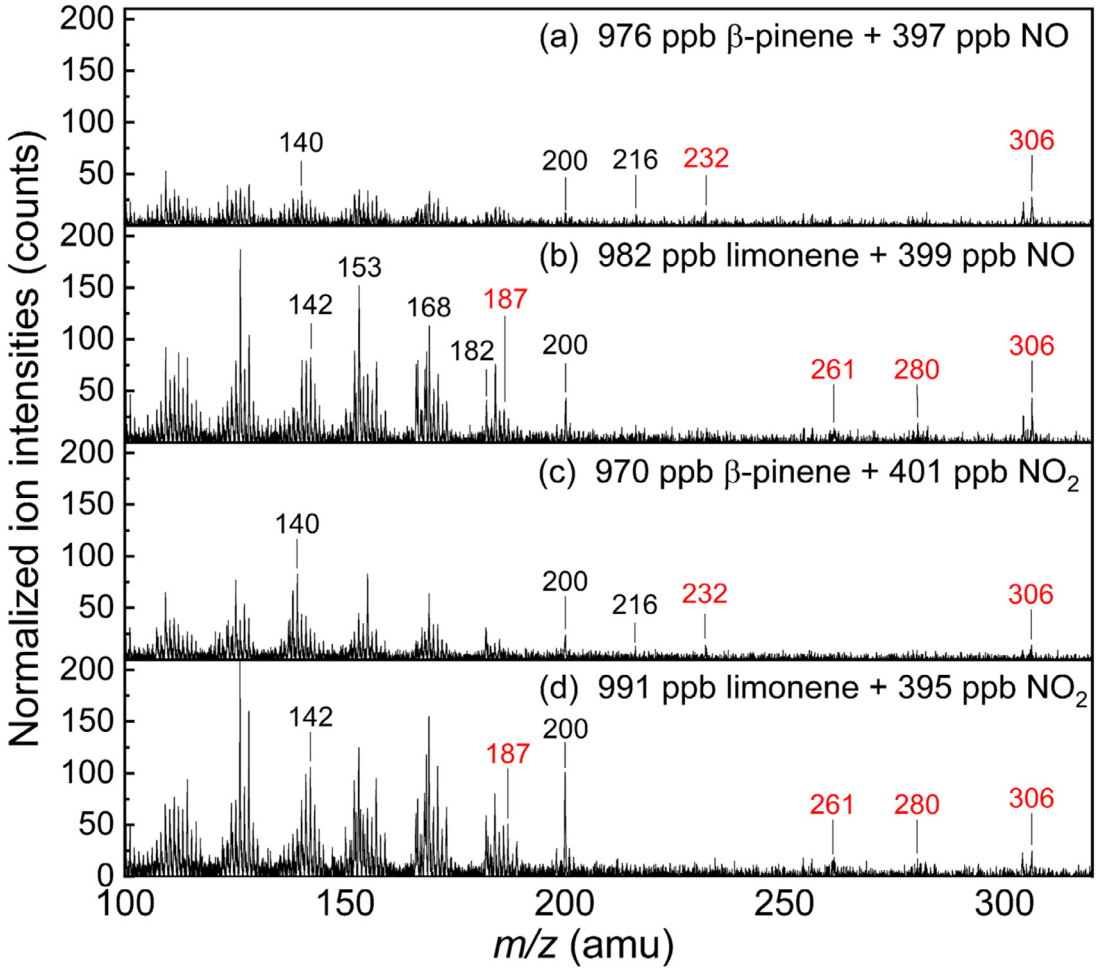

Fig. 6 – VUV-FEL photoionization mass spectra of the compounds generated under different experimental conditions. The compounds were ionized by the VUV-FEL at 125.0 nm. The newly-observed peaks are marked in red.

2025). In order to promote the beamtime efficiency of the expensive VUV-FEL, we prefer to employ VUV-FEL photoionization mass spectrometry to analyze these compounds under slightly higher concentrations than natural atmospheres.

2.3. *Characterization of chemical compositions during β-pinene and limonene photooxidation*

In this work, the VUV-FEL aerosol mass spectra were recorded every 5 min. Time point of maximum particle mass concentration was select to show the mass spectra in Fig. 6 as the SOA products. The number and intensities of mass spectral peaks of the compounds generated from limonene + NO/NO_2 photooxidation (Fig. 6b and d) are found to be significantly higher than those from β-pinene + NO/NO_2 (Fig. 6a and c), which complexity trend of chemical compositions supports the trend of particle mass concentrations and particle number concentrations (Figs. 1-4). The compounds observed at MW = 140, 168, 182, and 200 are consistent with the major products of β-pinene and limonene oxidation as previously determined by Fourier transform ion cyclotron resonance mass spectrometry (FT-ICR MS) and electrospray ionization mass spectrometry (ESI-MS) analysis (Huang et al., 2023; Liu et al., 2022). A new compound at MW = 306 is observed in all the photooxidation processes of β-pinene + NO/NO_2 and limonene + NO/NO_2. While a new compound at MW = 232 is observed in the β-pinene + NO/NO_2 photooxidation (Fig. 6a and c), three new compounds at MW = 187, 261, and 280 are observed in the limonene + NO/NO_2 photooxidation (Fig. 6b and d). The peak positions in the β-pinene + NO photooxidation (Fig. 6a) are similar to those of β-pinene + NO_2 photooxidation (Fig. 6c), with slightly higher intensities in the β-pinene + NO_2 photooxidation. A similar trend is observed for limonene + NO/NO_2 (Fig. 6b and d). This indicates that the relative abundance of NO and NO_2 in the atmosphere would affect the mass concentrations of SOA, but does not significantly alter the diversity of chemical compositions.

2.4. *Characterization of chemical compositions during β-pinene and limonene photooxidation*

In general, OH and O_3 (generated by NO_x photolysis) are the main oxidants for the VOC + NO_x photooxidation. Since the OH concentration is difficult to be precisely estimated under the current experimental conditions and O_3 has been demonstrated to play an important role in the VOC + NO_x photooxi-

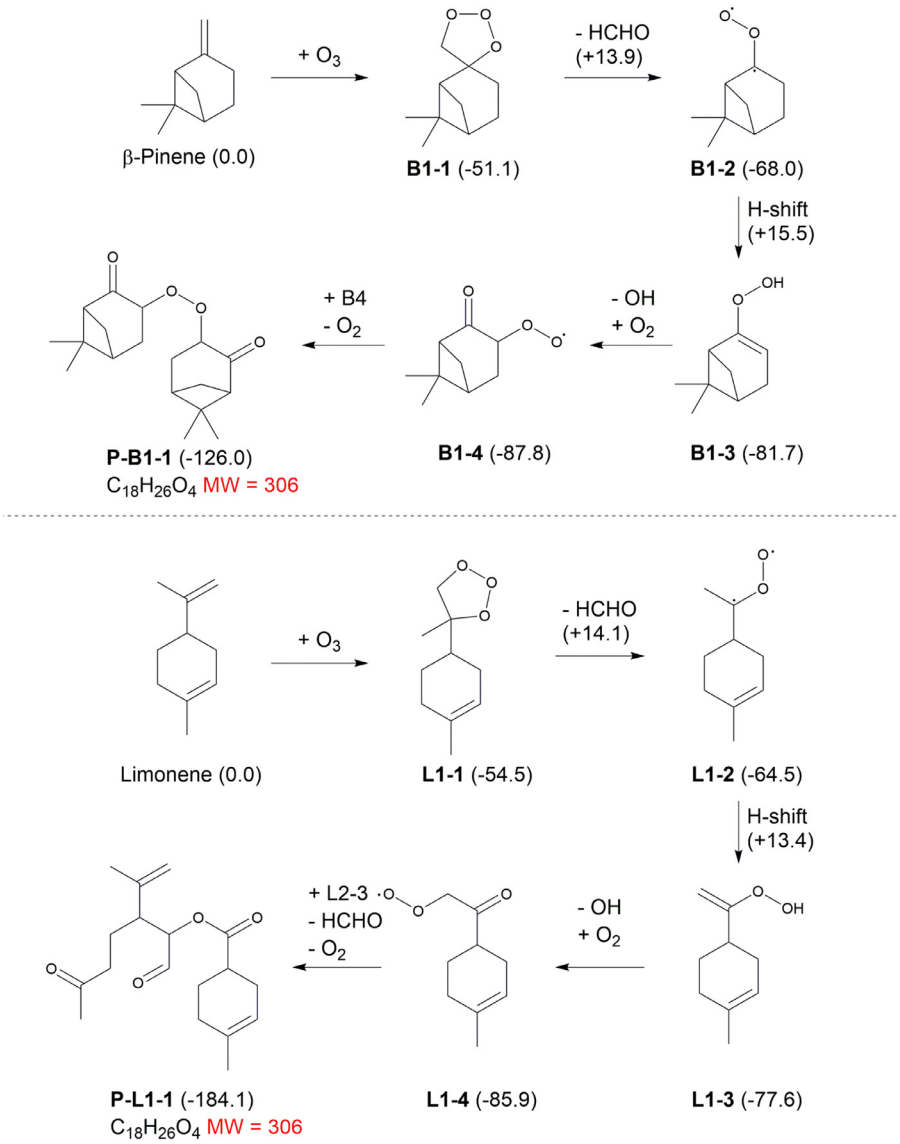

Fig. 7 – Reaction schematic of the RO_2–RO_2 reaction during the β-pinene + NO_x and limonene + NO_x photooxidation leading to the formation of C18 accretion products (MW = 306) calculated at the ωB97XD/def2-TZVP level of theory. Relative energies are given in kcal/mol.

dation (Kroll et al., 2005), O_3 is considered as the dominant oxidant in this work. Here, a combined approach using VUV-FEL photoionization mass spectrometry and theoretical calculations was employed to analyze the potential molecular structures and formation processes of monomers and dimers generated during the photooxidation of β-pinene and limonene. The potential formation mechanisms of the newly-observed species are depicted in Figs. 7 and 8, respectively, with a summary of molecular formulas in Appendix A Table S2. Appendix A Fig. S5 shows the main pathways initiated by O_3 for the photooxidation reactions of β-pinene and limonene. The products derived from β-pinene and limonene are designated as P-B*n*-*m* and P-L*n*-*m*, respectively, while the corresponding intermediates are denoted as B1-*n* and L1-*n* ordered by molecular weight.

Recent studies have underscored the significance of accretion reactions in the generation of low-volatility dimer compounds that serve as fundamental components of SOA formation (Berndt et al., 2018; Kenseth et al., 2023; Perakyla et al., 2023; Shi et al., 2022). However, limited information is available to the structural characteristics and formation mechanisms of accretion products, particularly those derived from different monoterpenes. In the atmospheric context, the RO_2 radicals engage in the accretion reactions, specifically manifested as $RO_2 + R'O_2 \rightarrow ROOR' + O_2$ and $R(CO)O_2 + R'O_2 \rightarrow R(CO)OR' + O_2$, leading to the formation of peroxide and ester accretion products. Fig. 7 shows the mechanisms for the generation of newly-observed products MW = 306 initiated from the ozonolysis of β-pinene and limonene. The terminal alkene functionality of β-pinene undergoes a reaction with O_3 to yield the primary ozonide (POZ) (B1–1), which is exothermic with a predicted value of 51.1 kcal/mol at the ωB97XD/def2-TZVP level of theory. B1–1 undergoes decomposition reaction (with the release of HCHO) to form B1–2, which is exothermic by 16.9 kcal/mol

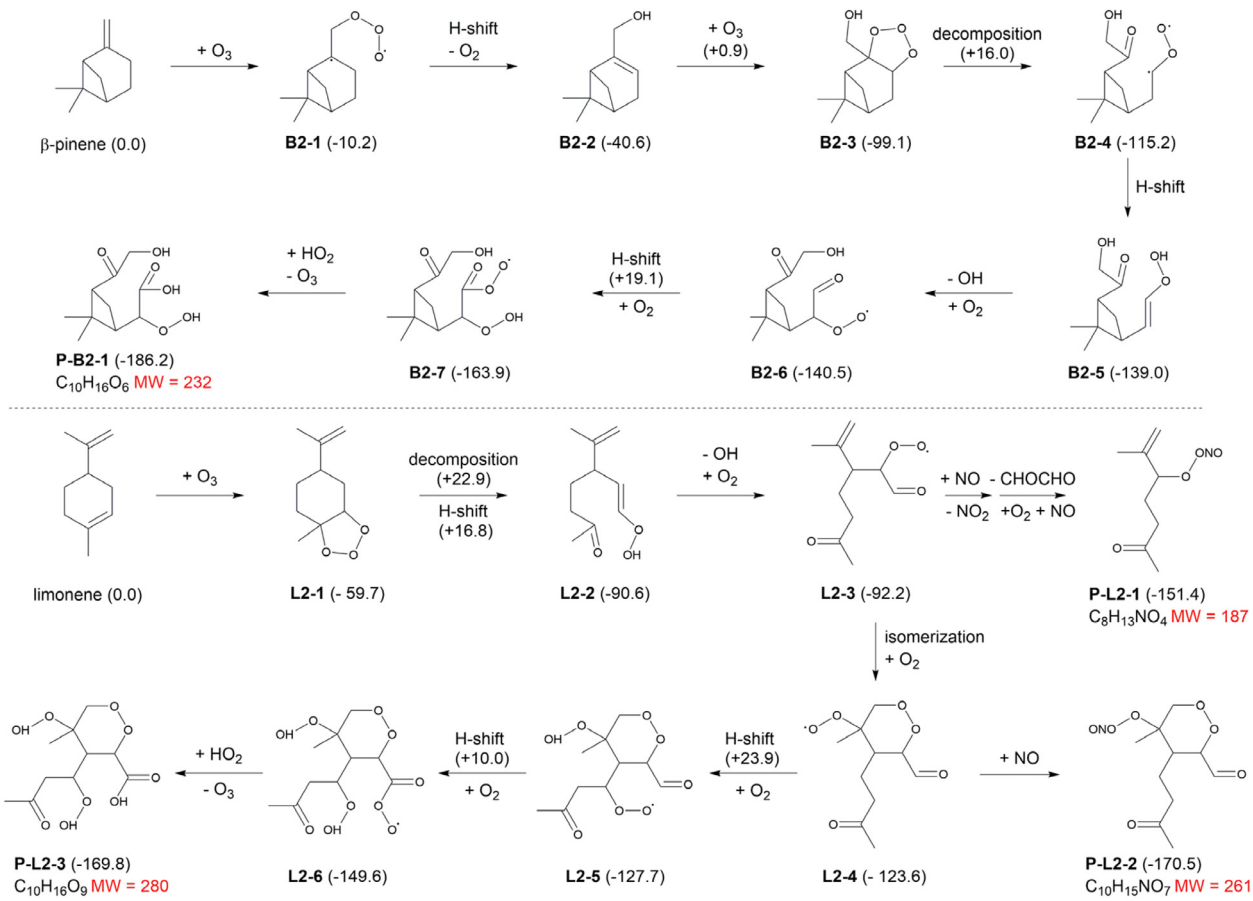

Fig. 8 – Autoxidation pathways of the β-pinene + NO_x and limonene + NO_x reactions calculated at the ωB97XD/def2-TZVP level of theory. Relative energies are given in kcal/mol.

and overcomes a barrier of 13.9 kcal/mol. B1–2 undergoes intramolecular H-shift to produce B1–3 with a predicted exothermicity of 13.7 kcal/mol and barrier of 15.5 kcal/mol. B1–3 releases OH and then reacts with O_2 to form B1–4 with a predicted exothermicity of 6.1 kcal/mol. The B1–4 → P-B1–1 (MW = 306) reaction is highly exothermic by 38.2 kcal/mol. Similar to the β-pinene → B1–4 process, the limonene → L1–4 process is also thermodynamically exothermic and dynamically feasible. In particular, the L1–4 → P-L1–1 (MW = 306) reaction for the limonene system (exothermic by 98.2 kcal/mol) is much more favorable than the corresponding reaction for the β-pinene system (exothermic by 38.2 kcal/mol). Previous research has shown that ester accretion products are generally less reactive and more stable than peroxide accretion products (Kenseth et al., 2023; Perakyla et al., 2023). Consequently, even though β-pinene and limonene undergo photooxidation to form compounds of the same molecular weight, limonene tends to yield ester dimeric accretion products, which is beneficial to the SOA formation with higher particle mass concentrations than β-pinene (Figs. 1-4). Establishing the chemical basis for formation of ester and peroxide accretion products helps to link the atmospheric degradation of different monoterpenes to the formation of low-volatility byproducts that can drive aerosol formation and growth.

Recent research has revealed that the monoterpene can rapidly produce large amounts of low-volatility vapors through gaseous autoxidation processes (Bianchi et al., 2019). With this clue, the possible formation routes for O_3 addition to the double bonds of β-pinene and limonene were explored by considering the potential reactions in the autooxidation pathway and the main results are shown in Fig. 8. The β-pinene → B2–2 process is exothermic with a predicted value of 40.6 kcal/mol, which aligns with previous results (Iinuma et al., 2007). Similarly, the B2–2 → B2–3 process is highly exothermic by 58.5 kcal/mol with an extremely low barrier of 0.9 kcal/mol. B2–3 is decomposed to form B2–4 with a predicted exothermicity of 16.1 kcal/mol and barrier of 16.0 kcal/mol. Similar to the B1–2 → B1–4 process, the B2–4 → B2–6 process is also exothermic with a predicted value of 25.3 kcal/mol. B2–6 undergoes intramolecular H-shift to form B2–7 with a predicted exothermicity of 23.4 kcal/mol and barrier of 19.1 kcal/mol. The B2–7 → P-B2–1 (MW = 232) reaction is exothermic by 22.3 kcal/mol. The limonene → L2–3 is substantially exothermic by 92.2 kcal/mol. The process from L2–3 to their corresponding product organic nitrates P-L2–1 (MW = 187) is facile with a calculated exothermicity of 59.2 kcal/mol. Due to the presence of the intramolecular double bond, L2–3 undergoes isomerization to form L2–4 with a predicted exothermicity of 31.4 kcal/mol. The L2–4 → P-L2–2 (MW = 261) reaction is feasible with a calculated exothermicity of 46.9 kcal/mol. L2–4 undergoes intramolecular H-shift and then reacts with O_2 to form L2–5 with a calculated

exothermicity of 4.1 kcal/mol and barrier of 23.9 kcal /mol. The L2–5 → L2–6 process is also feasible with a calculated exothermicity of 21.9 kcal/mol and barrier of 10.0 kcal/mol. The L2–6 → P-L2–3 (MW = 280) reaction is a favorable process with a calculated exothermicity of 20.2 kcal/mol.

3. Conclusion and implication

In this study, we investigated the individual effects of initial NO and NO_2 concentrations on the size distribution and particle mass concentration of SOA formed from the photooxidation of isomeric monoterpene, β-pinene and limonene. We further employed the VUV-FEL photoionization aerosol mass spectrometry to analyze the distinct chemical components of SOA. As compared to β-pinene, the SOA formed from the limonene photooxidation exhibits a higher particle number concentration and mass concentration and is more significantly influenced by the initial NO_x levels. For the β-pinene + NO_x photooxidation, a monotonous suppression effect of $[NO]_0$ on the particle mass concentration and a monotonous enhancement effect of $[NO_2]_0$ on the particle mass concentration is observed, respectively, which show significant correlation with the variation of cumulative amount of O_3 generated by NO_x photolysis. In contrast, for the limonene + NO_x photooxidation, a monotonous suppression effect of $[NO]_0$ on the particle mass concentration and a parabolic suppression/enhancement effect of $[NO_2]_0$ on the particle mass concentration is observed, respectively; as $[NO]_0$ gradually increases, the cumulative O_3 produced by NO_x photolysis exhibits a nonlinear trend, and there is no apparent correlation between the particle mass concentration and the accumulated O_3 concentration. Such difference of O_3 accumulation in the photooxidation reactions of different monoterpenes is consistent with the nonlinear variation of ground-level O_3 concentrations on NO_x levels (Chelani, 2010; Liu and Shi, 2021). Our laboratory studies confirm that NO_x influences the photochemical reactions leading to the formation of O_3 and SOA, substantiating its pivotal role in atmospheric oxidation capacity.

Using the advantages of high photoionization efficiency and wide wavelength modulation range of VUV-FEL, the photoionization mass spectra of SOA produced by the β-pinene and limonene photooxidation were detected to analyze their chemical compositions. A series of new compounds at MW = 232 and 306 formed from the β-pinene + NO_x photooxidation and those at MW = 187, 261, 280, and 306 formed from the limonene + NO_x photooxidation are identified, respectively. The MW = 306 (**P-B1–1 and P-L1–1**) compounds observed in the β-pinene + NO_x and limonene + NO_x photooxidation are generated by O_3 addition to the double bond and is assigned to peroxide and ester accretion product, respectively. The difference in the particle mass concentration and SOA yield for the β-pinene and limonene photooxidation may be ascribed to the diversity of product types formed through different oxidation pathways. The MW = 232 (**P-B2–1**), 187 (**P-L2–1**), 261 (**P-L2–2**) and 280 (**P-L2–3**) products are generated separately through autoxidation pathways of β-pinene and limonene. The observation of organic nitrates, MW = 261 (**P-L2–2**), resulting from limonene photooxidation, reflects the NO-inhibited effect on autoxidation pathway as observed in the experiments. This work underscores the significance of O_3 addition on the double bonds of β-pinene and limonene in the NO_x photooxidation process. Our findings reveal significant differences in the accretion products and HOMs formation derived from the photooxidation of β-pinene and limonene. The necessity to incorporate NO_x concentration-driven processes in the understanding of SOA formation and its dynamic evolution is a pressing concern in the context of future climate models, particularly in the neighborhood of emission origins.

Declaration of competing interest

The authors have no conflicts to disclose.

CRediT authorship contribution statement

Yingqi Zhao: Writing – original draft, Software, Methodology, Investigation, Formal analysis, Data curation. **Zhaoyan Zhang:** Investigation, Formal analysis, Data curation. **Ya Zhao:** Investigation, Formal analysis, Data curation. **Chong Wang:** Visualization, Investigation, Formal analysis, Data curation. **Hua Xie:** Validation, Methodology, Funding acquisition, Formal analysis. **Jiayue Yang:** Resources, Methodology. **Weiqing Zhang:** Resources, Methodology. **Guorong Wu:** Resources, Methodology. **Gang Li:** Writing – review & editing, Writing – original draft, Validation, Supervision, Project administration, Investigation, Funding acquisition, Formal analysis, Data curation, Conceptualization. **Ling Jiang:** Writing – review & editing, Writing – original draft, Visualization, Validation, Supervision, Project administration, Investigation, Funding acquisition, Formal analysis, Data curation, Conceptualization. **Xueming Yang:** Validation, Supervision, Project administration, Funding acquisition.

Acknowledgments

The authors gratefully acknowledge the Dalian Coherent Light Source (DCLS) and Specreation Co., Ltd. for support and assistance. This work was supported by the National Natural Science Foundation of China (Nos. 22125303, 92361302, 92061203, 22103082, 22273101, 22288201, and 21327901), the National Key Research and Development Program of China (No. 2021YFA1400501), the Innovation Program for Quantum Science and Technology (No. 2021ZD0303304), Dalian Institute of Chemical Physics (DICP I202437), Chinese Academy of Sciences (No. GJJSTD20220001), and the International Partnership Program of CAS (121421KYSB20170012).

Appendix A Supplementary data

Supplementary material associated with this article can be found in the online version at doi:10.1016/j.jes.2024.08.007.

References

Berndt, T., Scholz, W., Mentler, B., Fischer, L., Herrmann, H., Kulmala, M., et al., 2018. Accretion product formation from self- and cross-reactions of RO_2 radicals in the atmosphere. Angew. Chem. Int. Ed. 57, 3820–3824.

Berndt, T., Richters, S., Jokinen, T., Hyttinen, N., Kurtén, T., Otkjær, R.V., et al., 2016. Hydroxyl radical-induced formation of highly oxidized organic compounds. Nat. Commun. 7, 13677.

Bianchi, F., Kurten, T., Riva, M., Mohr, C., Rissanen, M.P., Roldin, P., et al., 2019. Highly oxygenated organic molecules (HOM) from gas-phase autoxidation involving peroxy radicals: a key contributor to atmospheric aerosol. Chem. Rev. 119, 3472–3509.

Bianchi, F., Trostl, J., Junninen, H., Frege, C., Henne, S., Hoyle, C.R., et al., 2016. New particle formation in the free troposphere: a question of chemistry and timing. Science 352, 1109–1112.

Byron, J., Kreuzwieser, J., Purser, G., van Haren, J., Ladd, S.N., Meredith, L.K., et al., 2022. Chiral monoterpenes reveal forest emission mechanisms and drought responses. Nature 609, 307.

Chelani, A.B., 2010. Nonlinear dynamical analysis of ground level ozone concentrations at different temporal scales. Atmos. Environ. 44, 4318–4324.

Chen, T., Zhang, P., Ma, Q., Chu, B., Liu, J., Ge, Y., et al., 2022. Smog chamber study on the role of NO_x in SOA and O_3 formation from aromatic hydrocarbons. Environ. Sci. Technol. 56, 13654–13663.

Crounse, J.D., Nielsen, L.B., Jørgensen, S., Kjaergaard, H.G., Wennberg, P.O., 2013. Autoxidation of organic compounds in the atmosphere. J. Phys. Chem. Lett. 4, 3513–3520.

Ehn, M., Thornton, J.A., Kleist, E., Sipilä, M., Junninen, H., Pullinen, I., et al., 2014. A large source of low-volatility secondary organic aerosol. Nature 506, 476–479.

Engelhart, G., Asa-Awuku, A., Nenes, A., Pandis, S., 2008. CCN activity and droplet growth kinetics of fresh and aged monoterpene secondary organic aerosol. Atmos. Chem. Phys. 8, 3937–3949.

Friedman, B., Farmer, D.K., 2018. SOA and gas phase organic acid yields from the sequential photooxidation of seven monoterpenes. Atmos. Environ. 187, 335–345.

Frisch, M., Trucks, G., Schlegel, H., Scuseria, G., Robb, M., Cheeseman, J., et al., 2016. Gaussian, 16. Gaussian. Inc., Wallingford, CT, USA.

Grosjean, D., Williams, E.L., Grosjean, E., Andino, J.M., Seinfeld, J.H., 1993. Atmospheric oxidation of biogenic hydrocarbons: reaction of ozone with β-pinene, D-limonene and trans-caryophyllene. Environ. Sci. Technol. 27, 2754–2758.

Guenther, A.B., Jiang, X., Heald, C.L., Sakulyanontvittaya, T., Duhl, T., Emmons, L.K., et al., 2012. The model of emissions of gases and aerosols from Nature version 2.1 (MEGAN2.1): an extended and updated framework for modeling biogenic emissions. Geosci. Model Dev. 5, 1471–1492.

Hallquist, M., Wenger, J.C., Baltensperger, U., Rudich, Y., Simpson, D., Claeys, M., et al., 2009. The formation, properties and impact of secondary organic aerosol: current and emerging issues. Atmos. Chem. Phys. 9, 5155–5236.

Hanson, D.R., Sawyer, A., Long, D., Sofio, D., Kunz, J., Wentzel, M., 2022. Particle formation from photooxidation of α-pinene, limonene, and myrcene. J. Phys. Chem. A 126, 910–923.

Huang, J.-H., Zhang, F., Shi, Y.-P., Cai, J.-R., Chuang, Y.-H., Hu, W.-P., et al., 2023. Water plays multifunctional roles in the intervening formation of secondary organic aerosols in ozonolysis of limonene: a valence photoelectron spectroscopy and density functional theory study. J. Phys. Chem. Lett. 14, 3765–3776.

Iinuma, Y., Müller, C., Berndt, T., Böge, O., Claeys, M., Herrmann, H., 2007. Evidence for the existence of organosulfates from β-pinene ozonolysis in ambient secondary organic aerosol. Environ. Sci. Technol. 41, 6678–6683.

Jimenez, J.L., Canagaratna, M.R., Donahue, N.M., Prevot, A.S.H., Zhang, Q., Kroll, J.H., et al., 2009. Evolution of organic aerosols in the atmosphere. Science 326, 1525–1529.

Jokinen, T., Sipilä, M., Richters, S., Kerminen, V.M., Paasonen, P., Stratmann, F., et al., 2014. Rapid autoxidation forms highly oxidized RO_2 radicals in the atmosphere. Angew. Chem. Int. Ed. 53, 14596–14600.

Kenseth, C.M., Hafeman, N.J., Rezgui, S.P., Chen, J., Huang, Y., Dalleska, N.F., et al., 2023. Particle-phase accretion forms dimer esters in pinene secondary organic aerosol. Science 382, 787–792.

Kirkby, J., Duplissy, J., Sengupta, K., Frege, C., Gordon, H., Williamson, C., et al., 2016. Ion-induced nucleation of pure biogenic particles. Nature 533, 521–526.

Kroll, J.H., Ng, N.L., Murphy, S.M., Flagan, R.C., Seinfeld, J.H., 2005. Secondary organic aerosol formation from isoprene photooxidation under high-NO_x conditions. Geophys. Res. Lett. 32, L18808.

Li, K.W., Chen, L.H., White, S.J., Han, K., Lv, B., Bao, K.J., et al., 2017. Effect of nitrogen oxides (NO and NO_2) and toluene on SO_2 photooxidation, nucleation and growth: a smog chamber study. Atmos. Res. 192, 38–47.

Liu, C., Shi, K., 2021. A review on methodology in O_3-NO_x-VOC sensitivity study. Environ. Pollut. 291, 118249.

Liu, D., Zhang, Y., Zhong, S., Chen, S., Xie, Q., Zhang, D., et al., 2022. Large differences of highly oxygenated organic molecules (HOMs) and low volatile species in SOA formed from ozonolysis of β-pinene and limonene. Atmos. Chem. Phys. 23, 1–29.

Luo, H., Vereecken, L., Shen, H., Kang, S., Pullinen, I., Hallquist, M., et al., 2023. Formation of highly oxygenated organic molecules from the oxidation of limonene by OH radical: significant contribution of H-abstraction pathway. Atmos. Chem. Phys. 23, 7297–7319.

McFiggans, G., Mentel, T.F., Wildt, J., Pullinen, I., Kang, S., Kleist, E., et al., 2019. Secondary organic aerosol reduced by mixture of atmospheric vapours. Nature 565, 587–593.

Nagori, J., Janssen, R.H.H., Fry, J.L., Krol, M., Jimenez, J.L., Hu, W., et al., 2019. Biogenic emissions and land-atmosphere interactions as drivers of the daytime evolution of secondary organic aerosol in the southeastern US. Atmos. Chem. Phys. 19, 701–729.

Normile, D., 2017. Unique free electron laser laboratory opens in China. Science 355, 235 -235.

Park, J.-H., Babar, Z.B., Baek, S.J., Kim, H.S., Lim, H.-J., 2017. Effects of NO_x on the molecular composition of secondary organic aerosol formed by the ozonolysis and photooxidation of α-pinene. Atmos. Environ. 166, 263–275.

Perakyla, O., Berndt, T., Franzon, L., Hasan, G., Meder, M., Valiev, R.R., et al., 2023. Large gas-phase source of esters and other accretion products in the atmosphere. J. Am. Chem. Soc. 145, 7780–7790.

Piletic, I.R., Kleindienst, T.E., 2022. Rates and yields of unimolecular reactions producing highly oxidized peroxy radicals in the OH-induced autoxidation of α-pinene, β-pinene, and limonene. J. Phys. Chem. A 126, 88–100.

Sarrafzadeh, M., Wildt, J., Pullinen, I., Springer, M., Kleist, E., Tillmann, R., et al., 2016. Impact of NO_x and OH on secondary organic aerosol formation from β-pinene photooxidation. Atmos. Chem. Phys. 16, 11237–11248.

Shen, H., Vereecken, L., Kang, S., Pullinen, I., Fuchs, H., Zhao, D., et al., 2022. Unexpected significance of a minor reaction pathway in daytime formation of biogenic highly oxygenated organic compounds. Sci. Adv. 8, 2375–2548.

Shi, X., Tang, R., Dong, Z., Liu, H., Xu, F., Zhang, Q., et al., 2022. A neglected pathway for the accretion products formation in the atmosphere. Sci. Total Environ. 848, 157494.

Shilling, J.E., Zaveri, R.A., Fast, J.D., Kleinman, L., Alexander, M.L., Canagaratna, M.R., et al., 2013. Enhanced SOA formation from mixed anthropogenic and biogenic emissions during the CARES campaign. Atmos. Chem. Phys. 13, 2091–2113.

Sillman, S., 1999. The relation between ozone, NO_x and hydrocarbons in urban and polluted rural environments. Atmos. Environ. 33, 1821–1845.

Tao, J., Zhao, C., Ma, N., Liu, P., 2014. The impact of aerosol hygroscopic growth on the single-scattering albedo and its application on the NO_2 photolysis rate coefficient. Atmos. Chem. Phys. 14, 12055–12067.

Tröstl, J., Chuang, W.K., Gordon, H., Heinritzi, M., Yan, C., Molteni, U., et al., 2016. The role of low-volatility organic compounds in initial particle growth in the atmosphere. Nature 533, 527–531.

Wang, T., Xue, L., Brimblecombe, P., Lam, Y.F., Li, L., Zhang, L., 2017. Ozone pollution in China: a review of concentrations, meteorological influences, chemical precursors, and effects. Sci. Total Environ. 575, 1582–1596.

Wang, X., Gidwani, A., Girshick, S.L., McMurry, P.H., 2005. Aerodynamic focusing of nanoparticles: II. Numerical simulation of particle motion through aerodynamic lenses. Aerosol Sci. Technol. 39, 624–636.

Wildt, J., Mentel, T.F., Kiendler-Scharr, A., Hoffmann, T., Andres, S., Ehn, M., et al., 2014. Suppression of new particle formation from monoterpene oxidation by NO_x. Atmos. Chem. Phys. 14, 2789–2804.

Wu, K., Yang, X., Chen, D., Gu, S., Lu, Y., Jiang, Q., et al., 2020. Estimation of biogenic VOC emissions and their corresponding impact on ozone and secondary organic aerosol formation in China. Atmos. Res. 231, 104656.

Xu, L., Yang, Z., Tsona, N.T., Wang, X., George, C., Du, L., 2021. Anthropogenic–biogenic interactions at night: enhanced formation of secondary aerosols and particulate nitrogen- and sulfur-containing organics from β-pinene oxidation. Environ. Sci. Technol. 55, 7794–7807.

Xu, L., Guo, H., Boyd, C.M., Klein, M., Bougiatioti, A., Cerully, K.M., et al., 2015. Effects of anthropogenic emissions on aerosol formation from isoprene and monoterpenes in the southeastern United States. Proc. Natl. Acad. Sci. U. S. A. 112, 37–42.

Xu, R., Thornton, J.A., Lee, B.H., Zhang, Y., Jaeglé, L., Lopez-Hilfiker, F.D., et al., 2022. Global simulations of monoterpene-derived peroxy radical fates and the distributions of highly oxygenated organic molecules (HOMs) and accretion products. Atmos. Chem. Phys. 22, 5477–5494.

Yee, L.D., Isaacman-VanWertz, G., Wernis, R.A., Kreisberg, N.M., Glasius, M., Riva, M., et al., 2020. Natural and anthropogenically influenced isoprene oxidation in southeastern United States and central Amazon. Environ. Sci. Technol. 54, 5980–5991.

Zang, X., Zhang, Z., Zhao, Y., Li, G., Xie, H., Zhang, W., et al., 2024. Effects of NO_2 and SO_2 on the secondary organic aerosol formation from beta-pinene photooxidation. J. Environ. Sci. 136, 151–160.

Zang, X., Zhang, Z., Jiang, S., Zhao, Y., Wang, T., Wang, C., et al., 2022. Aerosol mass spectrometry of neutral species based on a tunable vacuum ultraviolet free electron laser. Phys. Chem. Chem. Phys. 24, 16484–16492.

Zhang, H., Rattanavaraha, W., Zhou, Y., Bapat, J., Rosen, E.P., Sexton, K.G., et al., 2011. A new gas-phase condensed mechanism of isoprene-NO_x photooxidation. Atmos. Environ. 45, 4507–4521.

Zhang, Z., Zhao, Y., Zhao, Y., Zang, X., Xie, H., Yang, J., et al., 2024. Effects of NO and SO_2 on the secondary organic aerosol formation from isoprene photooxidation. Atmos. Environ. 318, 120248.

Zhang, Z., Zhao, Y., Zhao, Y., Zang, X., Xie, H., Yang, J., et al., 2025. Effects of isoprene on the ozonolysis of Δ^3-carene and β-caryophyllene: mechanisms of secondary organic aerosol formation and cross-dimerization. J. Environ. Sci. 150, 556–570.

Zhao, D.F., Schmitt, S.H., Wang, M.J., Acir, I.H., Tillmann, R., Tan, Z.F., et al., 2018. Effects of NO_x and SO_2 on the secondary organic aerosol formation from photooxidation of alpha-pinene and limonene. Atmos. Chem. Phys. 18, 1611–1628.